The conditions and specifications used for the experiment are listed in Table 1.

The CMOS point source image is deviated from the original light source with the distance d:

$$d = 2\theta f$$

$$\rightarrow d = \frac{2\theta f}{57.32} (\theta \text{ is angle})$$

$$\rightarrow \theta = \frac{28.66d}{f}$$

so we can get d from the collimator, and with d, we can calculate $\grave{e}$ from the earlier equation.

Ten samples were used for the experiment. Out of the 10 samples 3 are known to be out of specification with slope angle of greater than 1°. The experimental results are listed in Table 2.

We can see from earlier experimental results, samples #5, #8, and #10 has a $\grave{e}$ angle of greater than 1° confirming the presence of three samples that are out of specification

4. CONCLUSION

In conclusion, the experiment shows that the new method is a viable method for testing the parallel degree of CMOS image sensor bumping.

The advantages and disadvantages of this system are listed below:

The advantages are as follows:

1. Simple to operate.
2. Low cost.
3. Can be tested quickly, and is suitable for production.
4. Is a noncontact method for testing.
5. Full area testing versus point testing.

The disadvantages are as follows:

1. If the value of d is too small, it can easily result in measurement error.
2. All the modules in the system need to be extremely flat; otherwise it will cause the error.

In summary, although experimental results are in accordance with the theory, the samples tested are not enough validate this method for actual use. More sample testing is required to confirm the relevant data and accuracy.

TABLE 1 Conditions and Specifications Used for Experiment

Conditions	Specifications
Objective lens	Effective focal length (f) = 10 cm F/# = 2
Image sensor	30 million pixel CMOS image sensor; Pixel size: 5.6 μm × 5.6 μm; Sensitivity: 2.0 V/lux sec (555 nm); Array size: 3.6 mm × 2.7 mm
Distance from lens to the PCB	50 cm
Light sources	He-Ne laser (λ = 0.6328 μm)
Environmental intensity of illumination	550 lux
Pinhole	Diameter about 20 μm
Slope angle	$\theta < 1°$

TABLE 2 Experimental Results

Sample #	d (cm)	θ (Degree)
1	0.279	0.79
2	0.032	0.09
3	0.275	0.78
4	0.269	0.77
5	0.468	1.34
6	0.214	0.61
7	0.270	0.77
8	0.395	1.13
9	0.285	0.81
10	0.397	1.13

REFERENCES

1. J. Wilson and J. Hawkes, Optoelectronics, Prentice Hall, Upper Saddle River, NJ, 1998.
2. G.C. Holst, CCD arrays, cameras, and displays, 2nd ed, JCD Publishing, 1998.
3. R. Gregorian and G.C. Temes, Analog MOS integrated circuits for signal processing, Wiley, New York, NY, 1986.
4. M. Zhang, L. Liu, L. Wan, and Z. Luan, Wave-front analysis method of circular aperture sampling for collimation testing, Appl Opt 44 (2005), 2705-2709.
5. A. Anand and C.S. Narayanamurthy, Collimation testing using photore-fractive crystal and temporal coherence, Opt Eng 42 (2003), 1108–1113.
6. C. Shakher, S. Prakash, D. Nand, and R. Kumar, Collimation testing with circular gratings, Appl Opt 40 (2001), 1175–1179.
7. D.E. Silva, A simple interferometric method of beam collimation, Appl Opt 10 (1971), 1980–1982.

RAYLEIGH PARAMETER OF A ROUGH LAYER: APPLICATION TO FORWARD RADAR PROPAGATION OVER OIL SLICKS ON SEA SURFACES UNDER THE AMENT MODEL

Nicolas Pinel, Christophe Bourlier, and Joseph Saillard
IREENA Laboratory, La Chantrerie, BP 50609, 44306 Nantes Cedex 03, France

ABSTRACT: *The well-known Rayleigh parameter, which characterizes the degree of roughness of a corrugated surface for the case of reflection on a rough surface, is extended to the reflection on a rough layer. An application to the forward radar propagation over oil slicks on sea surfaces, using the Ament model, is given. © 2007 Wiley Periodicals, Inc. Microwave Opt Technol Lett 49: 2285–2290, 2007; Published online in Wiley InterScience (www.interscience.wiley.com). DOI 10.1002/mop.22716*

1. INTRODUCTION

In this article, the Rayleigh parameter is used to quantify the forward (i.e. in the specular direction) radar propagation over sea surfaces with the Ament model [1]. Indeed, the Ament model, which describes the forward radar propagation over a rough surface, is applied here to the propagation over clean and contaminated sea surfaces, for coastal radar configuration. This model based on a ray approach is a simple model, as it takes the surface roughness into account by multiplying the Fresnel reflection coefficient of a plane surface with the term $\exp(-2R_a^2)$ (for Gaussian statistics, with R_a the Rayleigh parameter), and does not take the shadowing effect into account [2]. Nevertheless, as shown in the literature [3], this simple model enables fast results, which are consistent with rigorous methods, for a ratio $\sigma_h/\lambda \lesssim 2$ (with λ the incident wavelength). This model is then very advantageous because for grazing angles, the rigorous methods, based on Methods of Moments, imply extensive computing time and memory space. The Ament model is then considered here for the extension to rough layers. In Section 2, the Rayleigh parameter for a single rough interface is presented. Then, it is extended in Section 3 to the case of a rough layer, and applied in Section 4 to the forward radar propagation over a rough layer under the Ament model.

2. RAYLEIGH PARAMETER FOR A SINGLE ROUGH INTERFACE

The Rayleigh parameter is a common notion that characterizes the degree of roughness of a corrugated surface. This parameter is inspired from Lord Rayleigh, who first worked on the scattering from rough surfaces [4]. It is expressed from the phase difference $\Delta\phi_r$ between the wave scattered in reflection from a point A of the rough surface, with coordinates (x_A, ζ_A), and a point of the mean plane $z = 0$ (plotted in gray dashed line, Fig. 1). This phase difference, which expresses the phase variation due to the surface roughness, is given for a surface of infinite extent by (Fig. 1)

$$\Delta\phi_r = 2k_1\Delta\zeta_A \cos\theta_i, \qquad (1)$$

where k_1 is the wave number inside the medium Ω_1, $\Delta\zeta_A = \zeta_A$ the height deviation of point A from the mean plane $z = 0$, and θ_i the incidence angle. The Rayleigh parameter $R_{a,r}$ (for the case of reflection from the rough surface) is then obtained from the root mean square of $\Delta\phi_r$. With zero mean height $\langle\Delta\zeta_A\rangle = \langle\zeta_A\rangle = 0$, $R_{a,r}$ is usually given by [5]

$$R_{a,r} = k_1\sigma_h \cos\theta_i, \qquad (2)$$
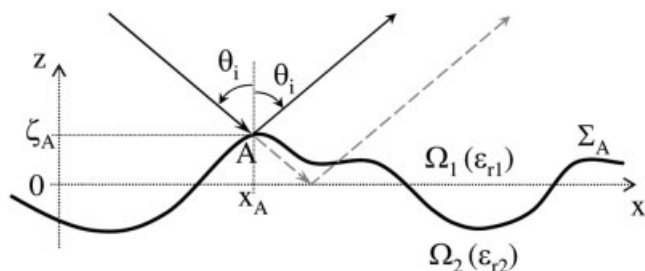
with σ_h the surface rms height.

Figure 1 Degree of roughness of a random rough surface: Reflection case
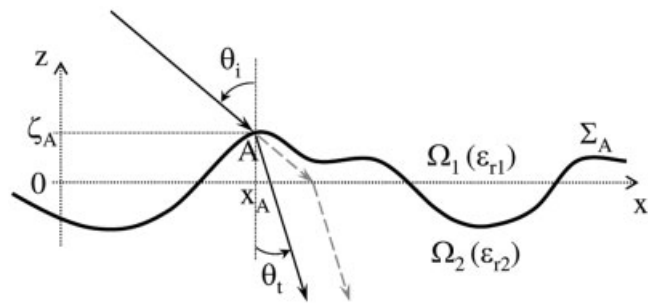

Figure 2 Degree of roughness of a random rough surface: Transmission case

2.1. Application to Forward Radar Propagation Over Sea Surfaces: Ament Model

Under the Ament model, the power scattered in reflection p_r from the rough surface is determined by the *coherent* power density p_r^{coh}, given by the expression $p_r^{coh} = |\langle E_r\rangle|^2/2Z_1$, with Z_1 the wave impedance and E_r the field scattered in reflection inside Ω_1. Then, the coherent power density for an infinite rough surface occurs in the specular direction (forward propagation), and differs from the one of an infinite plane surface by the multiplication of the term

$$|\langle\exp(j\Delta\phi_r)\rangle|^2 = \left|\int_{-\infty}^{+\infty}\exp(j\Delta\phi_r)p_h(\zeta)\,d\zeta\right|^2, \qquad (3)$$

where p_h is the surface height probability density function. For Gaussian statistics, it is equal to $\exp(-4R_{a,r}^2)$. Then, the Ament reflection coefficient r_A of the *field* scattered by the rough surface is defined as the product of the Fresnel reflection coefficient of a plane surface, r_{12} [6], with the phase variation term $\langle\exp(j\Delta\phi_r)\rangle$ such that [1]

$$r_A(\theta_i) = r_{12}(\theta_i)\int_{-\infty}^{+\infty}\exp(j\Delta\phi_r)p_h(\zeta)\,d\zeta. \qquad (4)$$

For Gaussian statistics, it is then equal to

$$r_A(\theta_i) = r_{12}(\theta_i)\exp(-2R_{a,r}^2). \qquad (5)$$

2.2. Extension of the Rayleigh Parameter to the Transmission Through the Surface

To extend the Ament reflection coefficient to the case of a rough layer, it is necessary first to define the Rayleigh parameter associated with the transmission of the wave through a rough surface. In parallel to the reflection case, the phase variation $\Delta\phi_t$ of the wave scattered in transmission due to the roughness is given by (Fig. 2)

$$\Delta\phi_t = k_0\Delta\zeta_A(n_1 \cos\theta_i - n_2 \cos\theta_t), \qquad (6)$$

with k_0 the wave number in the vacuum, θ_t the transmission angle, and n_1 and n_2 the refractive indexes of media Ω_1 and Ω_2, respectively. Similarly, the Rayleigh parameter $R_{a,t}$ for the transmission case is then given by

$$R_{a,t} = k_0\sigma_h\frac{|n_1 \cos\theta_i - n_2 \cos\theta_t|}{2}, \qquad (7)$$
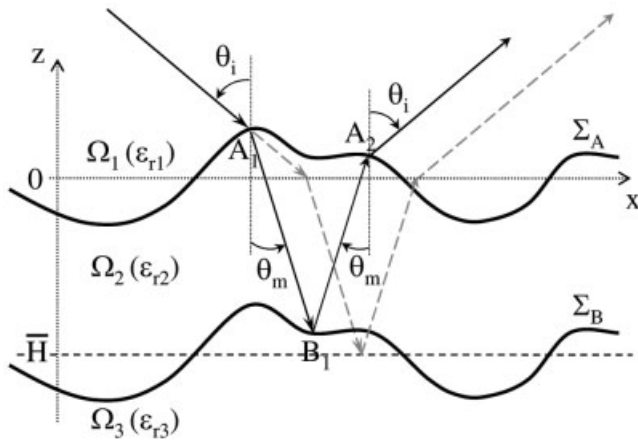
Figure 3 Degree of roughness of a random rough layer: Second-order contribution

where θ_t is related to θ_i by the Snell–Descartes law of a plane interface, $n_1 \sin \theta_i = n_2 \sin \theta_t$.

Let us note that contrary to the reflection case, where $R_{a,r}$ decreases when θ_i increases, for the transmission case, $R_{a,t}$ increases when θ_i increases. In other words, when θ_i increases, the rough surface is smoother for the reflection case and rougher for the transmission case. Then, when $\theta_i \rightarrow \pi/2$, $R_{a,r}$ tends to 0 and $R_{a,t}$ tends to

$$\lim_{\theta_i \rightarrow \pi/2} R_{a,t} = k_2 \sigma_h \cos \theta_t^l /2, \qquad (8)$$

with k_2 the wave number inside Ω_2, and $\theta_t^l = \arcsin(n_1/n_2)$ the limit refraction angle of a plane interface.

3. EXTENSION OF THE RAYLEIGH PARAMETERS TO A ROUGH LAYER

For the case of a rough layer (Fig. 3), the incident wave undergoes multiple successive reflections inside Ω_2, which induce an infinite number n of reflected fields inside Ω_1, E_1, E_2,... ,E_n. Then, a Rayleigh parameter $R_{a,1}$, $R_{a,2}$,... ,$R_{a,n}$ can be associated to the phase variations $\Delta\phi_1$, $\Delta\phi_2$,... ,$\Delta\phi_n$ of each scattered wave E_1, E_2,... ,E_n, respectively. For the first-order reflected field E_1, $\Delta\phi_1$ corresponds to the phase difference defined by Eq. (1):

$$\Delta\phi_1 = k_1 \Delta\zeta_{A_1} \cos\theta_i. \qquad (9)$$

For the second-order reflected field E_2 (Fig. 3), $\Delta\phi_2$ is calculated using the same way. It results from the scattering in transmission through the upper interface Σ_A, the scattering in reflection from the lower interface Σ_B, and then the scattering in transmission through Σ_A back into the incident medium Ω_1. Thus, it is given by the expression

$$\Delta\phi_2 = k_0 \Delta\zeta_{A_1}(n_1 \cos\theta_i - n_2 \cos\theta_m) + 2k_2 \Delta\zeta_{B_1} \cos\theta_m$$
$$+ k_0 \Delta\zeta_{A_2}(n_1 \cos\theta_i - n_2 \cos\theta_m), \qquad (10)$$

where $\Delta\zeta_{B_1} = \zeta_{B_1} + \bar{H}$ is the height deviation from the mean plane $z = -\bar{H}$ of the lower surface. Using the same way, the phase deviation $\Delta\phi_3$ of the third-order reflected field E_3 is given by

$$\Delta\phi_3 = k_0(\Delta\zeta_{A_1} + \Delta\zeta_{A_3})(n_1 \cos\theta_i - n_2 \cos\theta_m) + 2k_2(\Delta\zeta_{B_1} - \Delta\zeta_{A_2}$$
$$+ \Delta\zeta_{B_2}) \cos\theta_m. \qquad (11)$$

Similarly, $\Delta\phi_4$ of the fourth-order reflected field E_4 is given by

$$\Delta\phi_4 = k_0(\Delta\zeta_{A_1} + \Delta\zeta_{A_4})(n_1 \cos\theta_i - n_2 \cos\theta_m) + 2k_2(\Delta\zeta_{B_1} - \Delta\zeta_{A_2}$$
$$+ \Delta\zeta_{B_2} - \Delta\zeta_{A_3} + \Delta\zeta_{B_3}) \cos\theta_m, \qquad (12)$$

and so on for the higher orders.

Then, the first-order Rayleigh parameter $R_{a,1}$ associated to E_1 is given by Eq. (2) using $\sigma_h \equiv \sigma_{hA}$ the rms height of the upper surface. For uncorrelated surface points, the second-order Rayleigh parameter $R_{a,2}$ associated to E_2 is given by

$$R_{a,2}^2 = 2R_{a,t}^2 + R_{a,r3}^2, \qquad (13)$$

with $R_{a,t}$ given by Eq. (7) using $\sigma_h \equiv \sigma_{hA}$, and $R_{a,r3}$ by

$$R_{a,r3} = k_2 \sigma_{hB} \cos\theta_m, \qquad (14)$$

with $\sigma_h \equiv \sigma_{hB}$ the rms height of the lower surface. This can easily be generalized to any order $n \geq 2$ such that

$$R_{a,n}^2 = 2R_{a,t}^2 + (n-1)R_{a,r3}^2 + (n-2)R_{a,r2}^2, \qquad (15)$$

with

$$R_{a,r2} = k_2 \sigma_{hA} \cos\theta_m, \qquad (16)$$

4. APPLICATION TO THE AMENT EQUIVALENT REFLECTION COEFFICIENT OF A ROUGH LAYER

For the case of a layer of plane interfaces, the equivalent reflection coefficient r^{eq} [6] can be written in the form

$$r^{eq}(\theta_i) = r_{12}(\theta_i) + t_{12}(\theta_i)t_{21}(\theta_m) \times \sum_{k=0}^{\infty} r_{23}^{k+1}(\theta_m)r_{21}^k(\theta_m)e^{-j(k+1)\phi_{pl}},$$
$$(17)$$

with r_{ij} and t_{ij} the Fresnel reflection and transmission coefficients from the medium Ω_i to the medium Ω_j, respectively, and $\phi_{pl} = 2k_2\bar{H}\cos\theta_m$ the phase difference between E_1 and E_2. Owing to the roughness of both interfaces, one can define the Ament equivalent reflection coefficient r_A^{eq} as

$$r_A^{eq}(\theta_i) = r_{12}(\theta_i)\langle e^{j\Delta\phi_1}\rangle + t_{12}(\theta_i)t_{21}(\theta_m)$$

$$\times \sum_{k=0}^{\infty} r_{23}^{k+1}(\theta_m)r_{21}^k(\theta_m)e^{-j(k+1)\phi_{pl}}\langle e^{j\Delta\phi_{k+2}}\rangle. \qquad (18)$$

For uncorrelated surface points, the latter equation can be simplified. For Gaussian statistics, comparatively to the plane case where r^{eq} can be written as

$$r^{eq}(\theta_i) = \frac{r_{12}(\theta_i) + B}{1 + r_{12}(\theta_i)B}, \qquad (19)$$

with $B = r_{23}(\theta_m)e^{-j\phi_{pl}}$, $r_A^{eq}(\theta_i)$ can be expressed as

$$r_A^{eq}(\theta_i) = r_{12}(\theta_i)e^{-2R_{a,1}^2} + t_{12}(\theta_i)t_{21}(\theta_m)Be^{-2R_{a,2}^2}$$

$$\times \left[1 - \frac{r_{12}(\theta_i)B}{1 + r_{12}(\theta_i)Be^{-2(R_{a,r2}^2 + R_{a,r3}^2)}} \right], \qquad (20)$$

where the first term of the right-hand side of the equation, $r_{12}(\theta_i)e^{-2R_{a,1}^2}$, gives the Ament reflection coefficient of the upper interface.

4.1. Application to Forward Radar Propagation Over Oil Slicks on Sea Surfaces

This new Ament equivalent reflection coefficient is then applied to the forward radar propagation over sea surfaces covered in oil (called contaminated seas) and compared to clean sea surfaces. The calculations are performed at a frequency of 300 MHz ($\lambda = 1$ m) for a horizontally (H) polarized radar source. The complex relative permittivities of oil and seawater are then given by [7, 8]

$$\underline{\epsilon}_{r2} \simeq 2.25 + j0.01, \tag{21}$$

$$\underline{\epsilon}_{r3} \simeq 75 + j250, \tag{22}$$

respectively. The radar source is located at a fixed height $h_1 = 15$ m above the origin ($x_1 = 0$). The target or receiver is at an arbitrary altitude h_2, and is located at a range $x_2 = 2$ km away from the source (Fig. 4). The calculations are led for a wind speed at 10 m over the surface $u_{10} = 7$ m/s. Then, with the Elfouhaily et al. sea height spectrum [9], the sea surface rms height equals $\sigma_h^{\text{sea}} \simeq 0.32$ m. For a sea covered in oil, the height spectrum is modified by the oil slick. The Lombardini et al. height spectrum [10] is used here for a sea covered in oil, which depends on the characteristic pulsation ω_D and the elasticity modulus E_0 of the oil film. This model is independent of the oil layer thickness, and is valid for oil thicknesses of the order of a hundred micrometers to a millimeter.

Here, we consider a sea covered by an insoluble film. In Figure 5, the normalized height spectrum (isotropic part) of a contaminated sea surface, S_{cont}, is plotted versus the wave number k for $\{\omega_D = 6$ rad/s, $E_0 = 9$ mN/m$\}$ and $\{\omega_D = 11$ rad/s, $E_0 = 25$ mN/m$\}$. For comparison, the height spectrum (isotropic part) of a clean sea surface, S_{clean}, is plotted versus the wave number k using the Elfouhaily et al. spectrum [9]. These values were retrieved from experiments conducted in the Sicilian Channel and the Gulf of Maine [10]. The wind speed is $u_{10} = 7$ m/s. As expected, one can observe that the oil film strongly damps the high frequencies of the spectrum, which corresponds to the capillary waves of the surface. Moreover, the damping is stronger for $\{\omega_D = 11$ rad/s, $E_0 = 25$ mN/m$\}$ than for $\{\omega_D = 6$ rad/s, $E_0 = 9$ mN/m$\}$.

In what follows, we will take a characteristic pulsation $\omega_D = 6$ rad/s and a elasticity modulus $E_0 = 9$ mN/m for the oil slick. Then, for $u_{10} = 7$ m/s, the rms surface heights of both interfaces (i.e. air–oil and oil–sea interfaces) equal $\sigma_{hA} = \sigma_{hB} \simeq 0.29$ m.

To quantify the forward propagation over sea surfaces, the Ament model uses the propagation factor η, which is defined as the ratio of the field strength at the receiver reflected by the rough
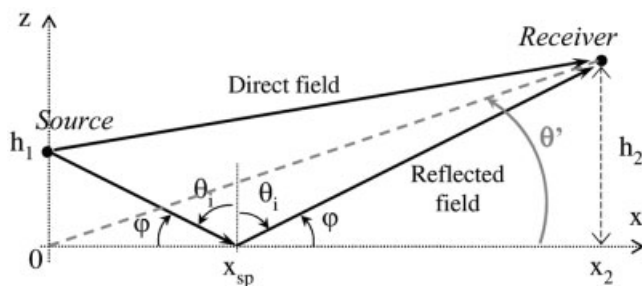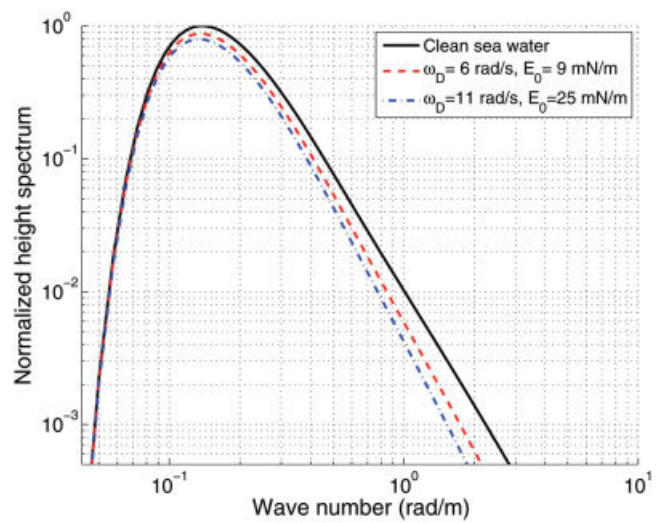

Figure 5 Normalized height spectrum (isotropic part) of clean and contaminated sea surfaces versus the wave number k. The wind speed is $u_{10} = 7$ m/s. [Color figure can be viewed in the online issue, which is available at www.interscience.wiley.com]

surface divided by the field strength at the receiver if it were in free space (direct field, Fig. 4). Then, the propagation factor η is given by the expression [3]

$$\eta = \sqrt{1 + |r|^2 + 2|r|\cos(k_1\delta + \angle r)}, \tag{23}$$

with $\angle r$ the phase of the reflection coefficient, and δ the path difference between the direct and reflected fields, which is given by

$$\delta = \frac{h_1 + h_2}{\sin\varphi} - \sqrt{(h_2 - h_1)^2 + x_2^2}. \tag{24}$$

4.2. Numerical Results

The numerical results present a comparison between a clean sea surface and a sea covered in oil, for the parameters quoted above. Figure 6 presents the propagation factor η in dB with respect to the height of the receiver h_2, for a range $x_2 = 2$ km. The clean sea surface is plotted in solid black line. For the sea covered in oil, the contribution of the first-order of the Ament equivalent reflection coefficient, $r_{12}\,e^{-2R_{a,1}^2}$, corresponding to the reflection from the air/oil interface, is plotted in red dashed line. The total Ament equivalent reflection coefficient r_A^{eq} is plotted in blue plus sign.

First, one can notice that the differences between the first-order and the total r_A^{eq} are negligible here. This implies that for this configuration, only the first-order of r_A^{eq} contributes to η. Indeed, for $h_2 \in [0; 180]$ m, the incidence angle $\theta_i > 84.4°$. Then, the reflection Rayleigh parameter $R_{a,r} \approx 0$, but the second-order Rayleigh parameter $R_{a,2}^2 \approx 6$, implying that $e^{-2R_{a,2}^2} \approx 0$. Thus, only the first order of r_A^{eq} contributes to η, and it would be necessary to work at lower frequencies so that the orders 2 and more can contribute to η. Then, for the typical applications presented here, the sea covered in oil can be taken into account by considering only the oil surface.

Moreover, the differences between the clean sea surface and the sea covered in oil are significant only around the minima or the maxima of the propagation factor η. The differences can be attributed to the differences in the rms surface heights, as well as the values of the Fresnel reflection coefficient $r_{12}(\theta_i)$, which differ

Figure 4 Forward propagation over rough surfaces: Configuration

owing to the contrast of the relative permittivities of the two media. Nevertheless, this contrast is low for this range of heights h_2, corresponding to a grazing angle θ' (Fig. 4): indeed, θ' ranges from 0° to 5.15°, which implies for $x_2 = 2$ km that θ_i ranges from 89.6° to 84.4°. Then, for very high θ_i, $r_{12}(\theta_i) \approx 1$, and the contrast increases when θ_i decreases (corresponding to increasing θ' and increasing h_2), as it can be seen in Fig. 6. This also means that the contrast increases for a lower range $x_2 < 2$ km: the detection of the oil slick is easier for low to moderate ranges x_2. As well, for higher heights h_2 of the receiver, corresponding to higher values of θ', this contrast increases.

Figure 7 presents the propagation factor η in dB with respect to h_2 for both H and V polarizations of the line source, with a wind speed $u_{10} = 10$ m/s. The clean sea surface is plotted in solid black line for H polarization and dash-dot blue line for V polarization. For the sea covered in oil, the contribution of the first-order of the Ament equivalent reflection coefficient, $r_{12}e^{-2R_{a,1}^2}$, corresponding to the reflection from the air/oil interface, is plotted in red dashed line for H polarization and green dotted line for V polarization. The total Ament equivalent reflection coefficient r_A^{eq} is plotted, only for V polarization, in green cross. Like for H polarization, which is not presented here, only the first-order of r_A^{eq} contributes to η for this configuration. For a wind speed $u_{10} = 10$ m/s, the rms height of the clean sea surface is $\sigma_h^{sea} \simeq 0.66$ m, and the ones for the contaminated sea are $\sigma_{hA} = \sigma_{hB} \simeq 0.62$ m.

For H polarization, as in the preceding configuration, the differences between the clean sea surface and the sea covered in oil are observable only around the minima or the maxima of the propagation factor η. The differences are a bit lower here for $u_{10} = 10$ m/s than for $u_{10} = 7$ m/s, owing to the lower dynamics of the sea curve. By contrast, for V polarization, one can observe a significant difference between the clean sea surface and the sea covered in oil: the dynamics of the curves and the positions of the extrema of the curves are different. This is due to the Brewster effect, which occurs only in V polarization. Indeed, the Brewster incidence angle θ_i^B for the loss-less sea surface ($\epsilon_{r3} = 75$) is $\theta_i^B \simeq 83.4°$, whereas the one for the lossless oil interface ($\epsilon_{r2} = 2.25$) is $\theta_i^B \simeq 56.7°$. Then, for the lossy media considered in Eqs. (21) and (22), the minimum of the absolute value of the reflection coefficient occurs for an incident angle close to θ_i^B. As h_2
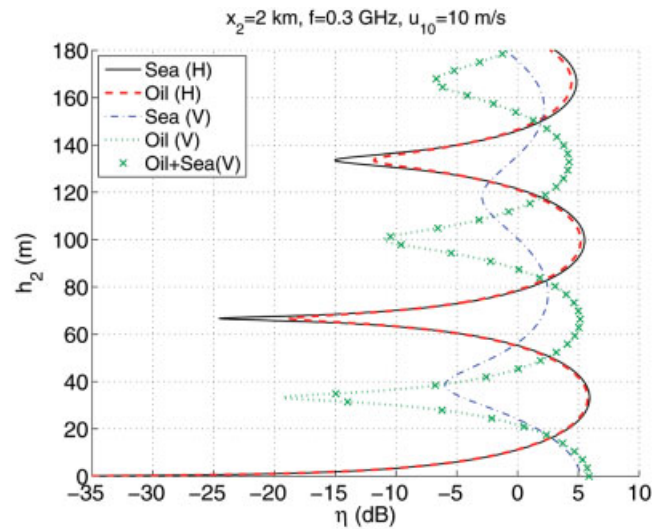

Figure 7 Comparison between a clean sea surface and a sea covered in oil for H and V polarizations, with $u_{10} = 10$ m/s. [Color figure can be viewed in the online issue, which is available at www.interscience.wiley.com]

ranges from 0 to 180 m, θ_i ranges from 89.6° to 84.4°: then, the reflection coefficient r_{12} is close to 0 for the sea surface and close to 1 for the air–oil interface. This accounts for the lower dynamics in η for the clean sea surface in comparison with the contaminated sea.

Moreover, the differences in the positions of the extrema between the clean and the contaminated sea for V polarization are due to the differences in the phase of the reflection coefficient $\angle r_{12}$ due to the Brewster effect. Indeed, for H polarization, $\angle r_{12} \in [-179.97°; -179.59°]$ for the sea surface and $[-180.00°; -179.96°]$ for the air–oil interface, whereas for V polarization, $\angle r_{12} \in [-128.10°; -8.33°]$ for the sea surface and $[-0.01°; -0.00°]$ for the air–oil interface.

Thus, the differences between the clean and the contaminated seas are much more significant for V polarization than for H polarization, allowing much easier detection of an oil slick.

5. CONCLUSION

In conclusion, the forward radar propagation over rough surfaces using the Ament model [3] has been extended to the case of rough layers, and applied to a sea covered in oil. A comparison between a clean sea surface and a sea covered in oil has been given. For the typical applications (microwave frequencies and coastal radar) presented, it is shown that only the first reflection from the air/oil interface contributes to the forward radar propagation over the rough layer. Then, for H polarization, the case of a sea covered in oil differs only from the clean sea surface by the contrast in permittivities, which induces a low to moderate contrast for grazing angles. This contrast is increased for lower ranges x_2 and higher heights h_2 of the receiver. By contrast, for V polarization, the case of a sea covered in oil differs from the clean sea surface owing to the Brewster effect, which contributes for the clean sea surface. This induces a high contrast in the positions and amplitudes of the extrema of the propagation factor, allowing easy oil slick detection.
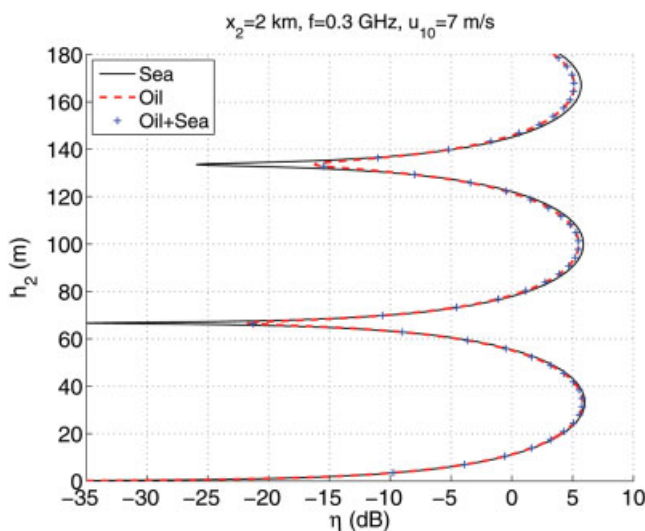

Figure 6 Comparison between a clean sea surface and a sea covered in oil for H polarization, with $u_{10} = 7$ m/s. [Color figure can be viewed in the online issue, which is available at www.interscience.wiley.com]

REFERENCES

1. W.S. Ament, Toward a theory of reflection by a rough surface, IRE Proc 41 (1953), 142–146.

2. V. Fabbro, C. Bourlier, and P.F. Combes, Forward propagation modeling above Gaussian rough surfaces by the parabolic wave equation: Introduction of the shadowing effect, Prog Electromagn Res 58 (2006), 243–269.

3. D.E. Freund, N.E. Woods, Hwar-Ching Ku, and R.S. Awadallah, Forward Radar propagation over a rough sea surface: A numerical assessment of the Miller-brown approximation using a horizontally polarized 3-GHz line source, IEEE Trans Antennas Propag 54 (2006), 1292–1304.

4. L. Rayleigh, On the dynamical theory of gratings, Proc R Soc Lond Ser A 79 (1907), 399–416.

5. J.A. Ogilvy, Theory of wave scattering from random surfaces, Institute of Physics Publishing, Bristol and Philadelphia, 1991.

6. M. Born and E. Wolf, Principles of optics, 6th ed., Pergamon, London, 1980.

7. F.T. Ulaby, R.K. Moore, and A.K. Fung, Microwave remote sensing: Active and passive, Vol. 3: From theory to applications, Artech House, Norwood, 1986.

8. T. Friizo, Y. Schildberg, O. Rambeau, T. Tjomsland, H. Fordedal, and J. Sjoblom, Complex permittivity of crude oils and solutions of heavy crude oils fractions, J Dispersion Sci Technol 19 (1998), 93–126.

9. T. Elfouhaily, B. Chapron, K. Katsaros, and D. Vandemark, A unified directional spectrum for long and short wind-driven waves, J Geophys Res 102 (1997), 781–796.

10. P.P. Lombardini, B. Fiscella, P. Trivero, C. Cappa, and W.D. Garrett, Modulation of the spectra of short gravity waves by sea surface films: Slick detection and characterization with a microwave probe, J Atmos Ocean Technol 6 (1989), 882–890.

Figure 1 Layout of a microstrip new compact dual-mode resonator (ground plane not shown)

COUPLINGS CONTROL IN A COMPACT MICROSTRIP DUAL-MODE RESONATOR

M. G. Banciu,[1] A. Ioachim,[1] R. Ramer,[2] N. Militaru,[3] and G. Lojewski[3]
[1]Microwave Group, National Institute of Materials Physics, 105 bis Atomistilor, Magurele, jud. Ilfov, 077125, Romania
[2]School of Electrical Engineering and Telecommunications, University of New South Wales, Sydney, New South Wales 2052, Australia
[3]Department of Telecommunications, Faculty of Electronics, Telecommunications and Information Technology, University "Politehnica" of Bucharest, 313 Spl. Independentei, 060042, Bucharest, Romania

ABSTRACT: *A compact microstrip dual-mode resonator with slots in the ground plane is presented in this paper. Several methods for coupling between the dual modes are investigated. One of the methods involves using slots in the ground plane in order to enhance the external coupling and to introduce the necessary perturbation to the initially symmetrical structure. The proposed device requires a surface area about 6 times smaller than the area needed for a conventional patch dual-mode resonator. © 2007 Wiley Periodicals, Inc. Microwave Opt Technol Lett 49: 2290–2295, 2007; Published online in Wiley InterScience (www.interscience.wiley.com). DOI 10.1002/mop.22722*

1. INTRODUCTION

Dual-mode filters are devices attractive to the telecommunication systems because of their compactness. Each dual-mode resonator contributes two poles to the overall frequency response. Since Wolff's pioneering work [1], the microstrip dual-mode filters have continuousl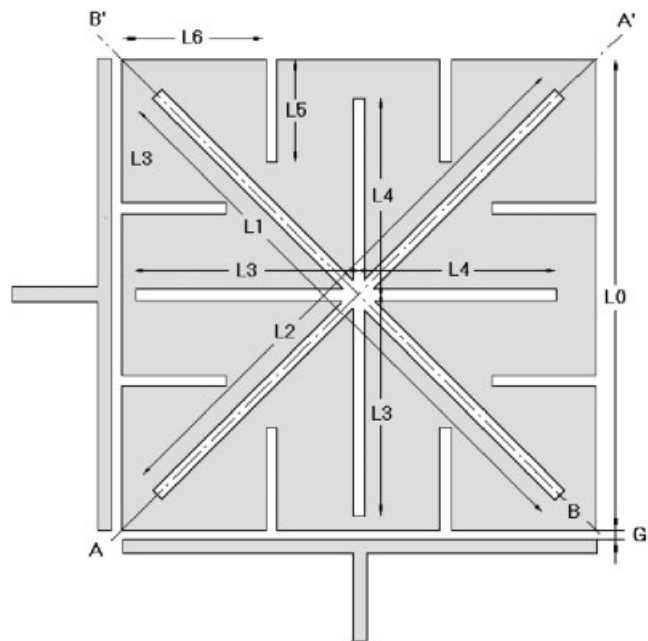y evolved [2–7]. The possibility of fabricating narrow pass-band filters by using low-loss high-temperature superconducting resonators advanced the interest for dual-mode filters [6, 7]. The superconducting patch resonators are particularly attractive in overcoming problems related to the critical surface current and in increasing the power handling capability [7].

Among the planar devices, the patch dual-mode filters offer low losses and very good power handling capability [7]. On the other hand, the loop dual-mode filters are more compact but provide less power handling capability. The new square patch dual-mode resonator proposed in this paper aims to combine the advantages of both closed loop and patch devices.

Several methods of coupling control between the orthogonal modes are investigated in this paper. Moreover, it is shown that the slots in the ground plane represent new and efficient means to control the external couplings.

2. CLOSED LOOP MODEL OF A NEW COMPACT DUAL-MODE FILTER

The new compact dual-mode resonator illustrated in Figure 1 is derived from a square patch dual-mode resonator. In this work, the microstrip device was developed on a $h_1 = 0.635$-mm-thick Rogers substrate with a $\varepsilon_{r1} = 10.8 \pm 0.25$ dielectric constant. When designed for 900 MHz, the dual-mode resonator had the dimension $L_0 = 20.5$ mm. Before introducing any perturbation to the symmetry, the length of the diagonal slots was $L_1 = L_2 = 24.61$ mm and the length of the nondiagonal slots was $L_3 + L_4 = 17.6$ mm. In addition, cuts of length $L_5 = 4.5$ mm were positioned at a distance $L_6 = 6.25$ mm from the corner. All slots and cuts in the microstrip patch have 0.5-mm slot width.

The substantial size reduction achieved by the proposed dual-mode resonator is due to the fact that the current is forced to follow a path of a quasifractal shape, rather than oscillate as in a conventional microstrip patch across the center of the square. Consequently, some of the filter properties could be understood by using a simple model of a closed-loop dual-mode resonator.